Biogeosciences, 12, 6869–6880, 2015
www.biogeosciences.net/12/6869/2015/
doi:10.5194/bg-12-6869-2015

Biogeosciences Open Access EGU

pH up-regulation as a potential mechanism for the cold-water coral *Lophelia pertusa* to sustain growth in aragonite undersaturated conditions

M. Wall[1,2], F. Ragazzola[3,a], L. C. Foster[3,b], A. Form[1], and D. N. Schmidt[3]

[1]GEOMAR Helmholtz Centre for Ocean Research, Kiel, Germany
[2]Alfred Wegener Institute for Polar and Marine Research, Bremerhaven, Germany
[3]School of Earth Sciences, University of Bristol, Bristol, UK
[a]now at: Institute of Marine Sciences, University of Portsmouth, Portsmouth, UK
[b]now at: Marine conservation society, Unit 3, Hereford and Worcester, UK

Correspondence to: M. Wall (mwall@geomar.de)

Received: 24 March 2015 – Published in Biogeosciences Discuss.: 5 May 2015
Revised: 2 November 2015 – Accepted: 22 November 2015 – Published: 1 December 2015

Abstract. Cold-water corals are important habitat formers in deep-water ecosystems and at high latitudes. Ocean acidification and the resulting change in aragonite saturation are expected to affect these habitats and impact coral growth. Counter to expectations, the deep water coral *Lophelia pertusa* has been found to be able to sustain growth even in undersaturated conditions. However, it is important to know whether such undersaturation modifies the skeleton and thus its ecosystem functioning. Here we used Synchrotron X-Ray Tomography and Raman spectroscopy to examine changes in skeleton morphology and fibre orientation. We combined the morphological assessment with boron isotope analysis to determine if changes in growth are related to changes in control of calcification pH. We compared the isotopic composition and structure formed in their natural environment to material grown in culture at lower pH conditions. Skeletal morphology is highly variable but shows no distinctive differences between natural and low pH conditions. Raman investigations found no difference in macromorphological skeletal arrangement of early mineralization zones and secondary thickening between the treatments. The δ^{11}B analyses show that *L. pertusa* up-regulates the internal calcifying fluid pH (pH_{cf}) during calcification compared to ambient seawater pH and maintains a similar elevated pH_{cf} at increased pCO_2 conditions. We suggest that as long as the energy is available to sustain the up-regulation, i.e. individuals are well fed, there is no detrimental effect to the skeletal morphology.

1 Introduction

The ocean is absorbing CO_2 from anthropogenic emissions resulting in a drop in carbonate saturation and ocean pH (Bates et al., 2012). Cold waters take up and store more CO_2 and thus the high latitudes will be amongst the first to experience undersaturated conditions (Orr et al., 2005). The response of marine calcifiers to ocean acidification has been shown to be taxon-specific (e.g. Ries et al., 2009; Pörtner et al., 2014); consequently, understanding the response of important key marine habitat builders is imperative to estimate potential impacts on their future ecosystem service. A large number of studies have concentrated on the physiological aspects of changes in carbonate chemistry (see Pörtner et al., 2014), much less is known about the impact this has on the skeleton grown by these organisms. While some species have been shown to continue to grow even under low pH conditions, a weakening of the ultra-structure can impair ecosystem functionality, i.e. its ability to withstand predators and wave action (Chan et al., 2012; Ragazzola et al., 2012; Melbourne et al., 2015).

Cold-water corals are important habitat builders that offer a range of microhabitats sustaining high biodiversity and provide nursery grounds for various species of fish (Fosså et al., 2002; Henry and Roberts, 2007; Roberts et al., 2008). The maintenance of their structural integrity is essential not just for the species itself but also for a wide range of species which depend on this habitat. *Lophelia pertusa* is the most

common species of cold-water corals and has a cosmopolitan distribution with a wide temperature (4–12 °C) and salinity range (35–37 psu) suggesting a relatively high tolerance to environmental drivers. The species is typically found in regions with strong water currents and high productivity (Genin et al., 1986; Mienis et al., 2007). The modern distribution of cold-water corals appears to be constrained by the aragonite saturation horizon (the depth below which the waters become undersaturated with respect to aragonite), with 88.5 % of all cold-water coral records found above the aragonite saturation horizon (Davies and Guinotte, 2011; Guinotte and Fabry, 2008). Importantly for their future distribution, the aragonite saturation horizon has shoaled by 80–400 m in the North Atlantic since the industrial revolution (Feely et al., 2004) and model projections suggest a shoaling of up to 2000m by the end of this century resulting in vast areas of their current habitat being undersaturation with regards to aragonite (Orr et al., 2005).

Despite the strong link between the distribution of cold-water corals and the aragonite saturation horizon, *Lophelia pertusa* can calcify in undersaturated conditions (Form and Riebesell, 2012; Hennige et al., 2014; Maier et al., 2009, 2012), likely facilitated by its ability to increase the internal calcifying fluid pH at the site of calcification (pH_{cf}), termed "up-regulation". Most indications for up-regulation come from indirect determinations, e.g. measuring the boron isotopic composition ($\delta^{11}B$) of bulk skeleton samples of corals (Anagnostou et al., 2012; Holcomb et al., 2014; McCulloch et al., 2012; Trotter et al., 2011). Measurement of the pH_{cf} at the site of calcifications in several corals confirmed an ability of the organism to influence the internal pH_{cf} with a range of physiological processes (Al-Horani, 2003; Ries, 2011; Venn et al., 2013). The skeletal $\delta^{11}B$ was observed to decrease with lower saturation state and pH of seawater (in total scale: pH_T), suggesting a relative lowering of the internal pH_{cf} in response to external pH decrease. At low seawater pH_T, internal pH_{cf} is still significantly higher than seawater pH_T (up-regulation intensity, where $\Delta pH = pH_{cf} - pH_T$, Anagnostou et al., 2012; McCulloch et al., 2012; Trotter et al., 2011), but does not reach internal pH_{cf} levels observed under control conditions (Holcomb et al., 2014; Trotter et al., 2011).

This up-regulation ability has several implications: firstly, the potential to moderate the impact of projected future saturation state depends on the strength and efficiency of this mechanism (less efficient up-regulating species may be more adversely affected). Secondly, such differences in efficiencies will affect the reliability of $\delta^{11}B$ as pH proxy when applied to paleo-climate reconstruction. Thirdly, the establishment of a pH gradient between external seawater and internal site of calcification requires energy reallocation (Al-Horani et al., 2003; Chalker and Taylor, 1975) and altered energetic demands may affect skeletal structure and strength.

In order to understand the interaction of biomineralization response, we analysed *L. pertusa* skeletons grown under natural control (Sula Reef $pCO_2 = 405$ µatm) and elevated CO_2 conditions (CRSIII $pCO_2 = 982$ µatm). We uniquely combined Raman spectroscopy, Secondary Ionisation Mass Spectrometry (SIMS) and Synchrotron X-Ray Tomographic Microscopy (SXRTM) to examine whether ocean acidification causes any change in skeletal morphology of *L. pertusa*, such as thickness and growth patterns, or in the biomineralization processes. SIMS $\delta^{11}B$ transects are compared between the high pCO_2 (CRSIII) treatment and the natural conditions (Sula Reef). The $\delta^{11}B$ are converted to pH_{cf} to examine potential physiological adjustments in coral biomineralization under anticipated future ocean conditions of lower pH_T.

2 Material and methods

2.1 Specimens

The *Lophelia pertusa* specimens are grown in an experimental set-up at GEOMAR, Germany (see Form and Riebesell, 2012 for full details about the experimental set-up). In brief, the live branches of *L. pertusa* were collected with minimal invasion using the manned submersible JAGO at the central part of the Sula Reef complex (64°06′ N, 8°05′ E) off the Norwegian coast in 2008. The samples were transferred to Kiel and after a 3-month acclimatization period they were stained using Alizarin Red S (Standard Fluka: Sigma-Aldrich, Steinheim, Germany, with a concentration of 5 mg L^{-1} for an incubation period of 8 days to mark the start of the experiment). The corals were kept at a constant temperature (7.5 °C) and salinity (34.5 psu) similar to the conditions at the Sula Reef. After staining, the corals were transferred to the treatment tanks and the pCO_2 was over 2 weeks gradually adjusted to the treatment conditions which are summarized in Table 1. The specimens were cultured for 6 months in all treatments. SIMS $\delta^{11}B$ transects and Raman are compared between the high pCO_2 (CRSIII) treatment and the natural conditions (Sula Reef), while for SRXTM and wall thickness measurements individuals from all treatments were used (CRSI $pCO_2 = 605$, CRSII $pCO_2 = 778$ and CRSIII $pCO_2 = 982$ µatm).

Cold-water corals show isotopic (including $\delta^{11}B$) and elemental heterogeneities within the early mineralizing skeleton (including EMZ like structure in the theca wall, e.g. Adkins et al., 2003; Blamart et al., 2007). To overcome this heterogeneity, studies using cold-water corals to trace seawater pH_T limit the sampling to the outer thecal wall and integrate large skeletal areas (e.g. McCulloch et al., 2012; Anagnostou et al., 2012). Main growth occurs at the polyp tip, where the theca wall is very thin and predominately formed by primary skeleton. This area is normally avoided in boron studies as it is calcified under a different mechanism than the secondary theca thickening.

Cold-water corals grow slowly which makes it impossible for us to follow this approach. It would also limit our analysis

Table 1. Summarized environmental and culturing conditions from Form and Riebesell (2012) applicable to the specimens and skeletal regions analysed for skeletal boron isotopic composition.

	Sula reef	Cultured CRSIII
Temperature (°C)	7.5	7.5 ± 0.1
alinity (PSU)	35.2	34.5 ± 0.5
Depth (m)	285	n/a
Total alkalinity ($\mu mol\,kg^{-1}$)	2313.7	2349.9 ± 79.5
DIC ($\mu mol\,kg^{-1}$)	2149.8	2300.1 ± 89.2
pH_{ext} (in total scale)	8.02	7.72 ± 0.056
pCO_2 (µamt)	405	982 ± 146
HCO_3^-	2009.3	2192.3 ± 87.0
Ω_{Ar}	1.74	0.932 ± 0.097

to a part of the skeleton and not allow the more holistic look at the growth we would like to achieve. To evaluate the $\delta^{11}B$ change with changing seawater conditions and to be able to link this directly to structural material analysis, a high-spatial resolution technique was applied to material that was grown during the culturing period. To separate the growth of the skeleton during natural and treatment conditions, we traced the Alizarin staining line. In the theca wall where growth is slower Alizarin was incorporated in traces and we used Raman spectroscopy to determine the start of the experiments.

For Raman and SIMS analyses, specimens cultured in the high treatment (982 ± 146 µatm) were compared to branches and/or skeletal regions grown naturally in the field. The specimens were cut transversal (at different heights along the corallite) and longitudinal. From the high pCO_2 treatment (CRSIII) one polyp was cut above and below the Alizarin stain (Fig. 1b) and another polyp was cut transversally through the thecal wall. The sample preparations allow a comparison of skeleton grown naturally in situ to pre-study conditions and during the culturing time prior to the staining as well as the treatment conditions after staining.

2.2 Raman mapping

Raman mapping was done using a WITec alpha 300 R (WITec GmbH, Germany) Confocal Raman Microscope equipped with an ultra-high throughput spectrometer (UHTS 300, WITec, Germany) and an EMCCD camera (grating of 600 grooves mm^{-1}, blazed at 500 nm and centred at 2400 cm^{-1}). Laser excitation wavelength of 488 nm was used. Raman maps were derived using a Nikon 20× (numeric aperture (NA) = 0.4) objective for large area scans and a Nikon 100× (NA = 0.9) for small high-resolution area scans. The spectra during mapping were recorded with an integration time of 35 ms and a step size of 1 µm (large area scans) and 10 ms and 0.5 µm for small area scans. The symmetric stretch of the carbonate (1085 cm^{-1}) provides information on the crystal orientations and was used to map the skeletal growth patterns and arrangement. Fluorescence intensity distribution (in the spectral range between 2400–2700 cm^{-1}) was used as a proxy to map organic matrix distribution within biogenic minerals (Wall and Nehrke, 2012) as well as to map the location of the staining line where it was not visible in microscopic images. All Raman spectral data sets were processed using the WITec Project software (version 2.04, WITec GmbH, Germany).

Transversal sections of *L. pertusa* calices show differences in skeletal densities (Fig. 1a) visible as differences in opaqueness of the skeleton. This criterion is often used to determine growth rings and to identify nucleation zones, which are characterized by distinct elemental ratios and isotopic signatures (Mortensen and Rapp, 1998; Wainright, 1964) compared to the bulk thecal skeleton (Adkins et al., 2003; Blamart et al., 2007; Cohen et al., 2006). Confocal Raman maps of the aragonite symmetric stretch intensity (the intensity of the main carbonate peak) allows similarly to distinguish the different skeletal regions (for detailed information see Wall and Nehrke, 2012). Here, skeletal regions were divided into a primary skeleton around the central corallite line (composed of EMZ) and paralleled layered fibre growth, giving the corallites their shape and size. A secondary thickening is subsequently responsible for the addition of skeletal mass to the corallite theca (Fig. 1e). The growth patterns within primary and secondary skeleton are compared between natural conditions and the treatments and used to relate the boron isotopic signature to the different growth stages.

2.3 $\delta^{11}B$ with SIMS

Boron isotopes in marine biogenic carbonates are a pH-proxy, which varies systematically with seawater pH (e.g. Hemming and Hanson, 1992; Rae et al., 2011). The value recorded depends on a strong biological control ("vital effect") and reflects internal calcifying fluid pH_{cf} (Hönisch et al., 2004; Holcomb et al., 2014; McCulloch et al., 2012). The following equation converts $\delta^{11}B$ into pH (or pH_{cf}):

$$pH = pK_B^* - \log\left[\frac{\delta^{11}B_{sw} - \delta^{11}B_C}{\alpha_B \times \delta^{11}B_C - \delta^{11}B_{sw} + 1000 \times (\alpha_B - 1)}\right] \quad (1)$$

pK_B^* = dissociation constant of boric acid (Dickson, 1990). The theoretical $\delta^{11}B$ for the sample location can be calculated using $pK_B^* = 8.795$ for the natural in situ grown skeletal and $pK_B^* = 8.814$ for the treatment specimen. pK_B^* values were calculated from seacarb using the software package R (Lavigne and Gattuso, 2010).

α_B = isotopic fractionation factor in seawater at 25°C is 1.0272 ± 0.0006 (Klochko et al., 2006).

$\delta^{11}B_{sw}$ = boron isotope composition of seawater is 39.61 ‰ (Foster et al., 2010).

$\delta^{11}B_C$ = measured $\delta^{11}B$ of the studied coral specimen.

For SIMS measurements we used the Cameca-ims-f4 and the Cameca-ims-1270 at the EMMAC facility, University of Edinburgh with the following measuring procedure: the sections were gold-coated and analysed with a $^{16}O_2^-$ primary

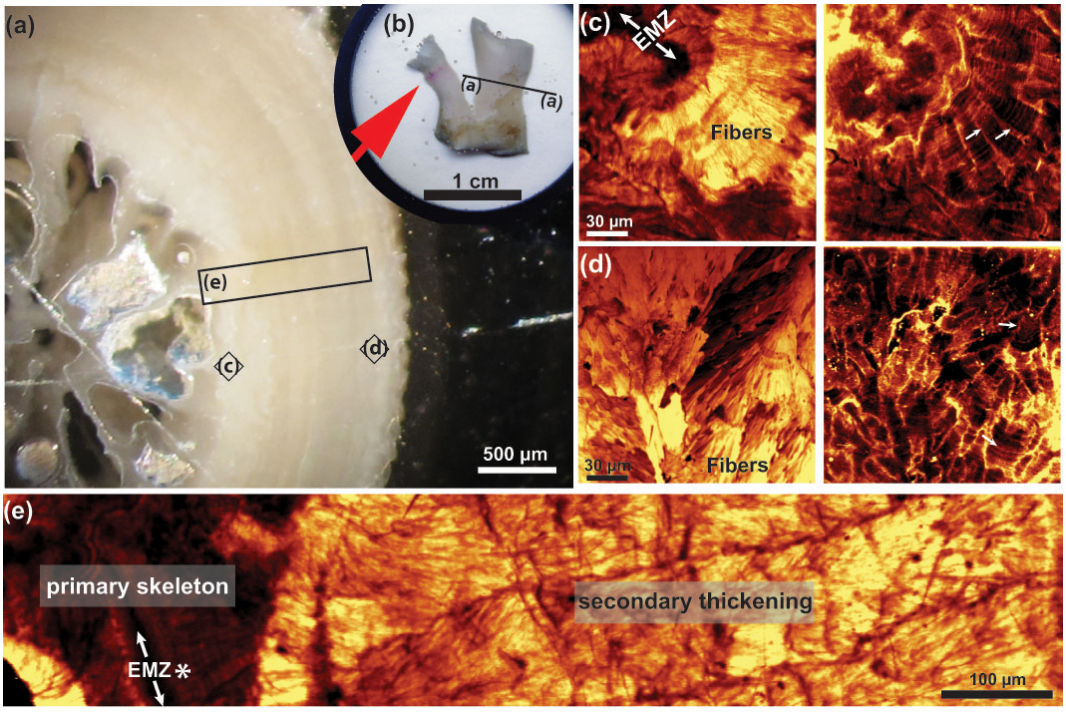

Figure 1. *Lophelia pertusa* colony **(a)** cut in transversal plane of an old branch and **(b)** *Lophelia* colony cut in longitudinal plane with two branches (old and a young branch). The young side branch shows the Alizarin stain. **(c, d)** Raman maps of aragonite fibre orientation (left map) and fluorescence (right map) within the primary skeleton with early mineralization zone (EMZ; **c**) and within the secondary thickening **(d)**. The arrows in **(c, d)** mark skeletal organic matrix bands. **(e)** Raman maps of aragonite fibre orientation clearly differentiating primary skeleton and secondary thickening of the corallite and early mineralization zone (EMZ).

beam. For the f4 the primary beam energy was 15 keV and a beam current between 10 and 40 nA to produce positive secondary ions of 10B+ and 11B+ and for the 1270 a primary beam energy of 12.2 keV and secondary ion energy of 10 keV resulting in a net primary impact energy of 22 keV. The secondary ions were analysed with an energy window of 52 eV, a 150 µm image field using 450 µm contrast and 1800 µm field apertures. Surface contamination was minimized using a 30 s pre-sputter, Köhler illumination with a field aperture limiting ions to the central area of the sputter pit. The isotope ratio was measured for 200 cycles for the f4 and 60 cycles for the 1270 per spot analysis, each cycle consisting of 5 and 3 s integrations of 10B+ and 11B+ respectively. The beam diameter at the end of the analysis was ∼ 25 by 40 µm. For details see Kasemann et al. (2009). Analyses followed line-transects and single spots were spaced ∼ 30–50 µm apart (depending on the sampling location). A minimum of 10 spot analyses of the internal standard M93 coral bulk standard (Kasemann et al., 2009, 24.8 ± 0.4 ‰ (2SD)) was run each day of analyses on both instruments, with an average of 3.79 ± 0.44 ‰ (1SE) and used to normalize sample ^{11}B / ^{10}B values.

We analysed three colonies from Sula reef to assess the variability within the population. We tested how representative our cross sections are by analysing two sections from the same corallite. We also tested reproducibility of our results by comparing two corallites from the same coral colony and then compared growth prior to staining with material grown in culture (for schematic representation see Supplement Fig. S1).

2.4 Synchrotron analyses and wall thickness changes

Synchrotron-based X-ray Tomographic Microscopy were performed at the TOMCAT beamline at the Swiss Light Source, Paul Scherrer Institut, Villigen, Switzerland (Stampanoni et al., 2006). One specimen from each of the CO_2 levels was scanned (CRSI-CRSIII: 604 ± 105, 778 ± 112 and 982 ± 146 µatm). For each tomographic scan, 377 projections over 180 degrees were acquired at energy of 28 keV with UPLAPO 2× objective (field view of 7.5 × 7.5 mm^2; pixel size 3.7 × 3.7 mm^2). The exposure time was 250 ms. Further processing was done using Avizo to produce 3-D isosurface model and measure sample thickness above and below Alizarin stain lime (Fig. 2b) by cross-referencing to the sample. In addition, longitudinal cuts of *Lophelia pertusa* polyps (n = 5–7, per treatment) grown at the distal ends of the colonies were analysed with a microscope to measure wall thickness below and above the staining line. The thickness ratio of below and above staining line was calculated and compared between treatments. Polyp diameter is not cor-

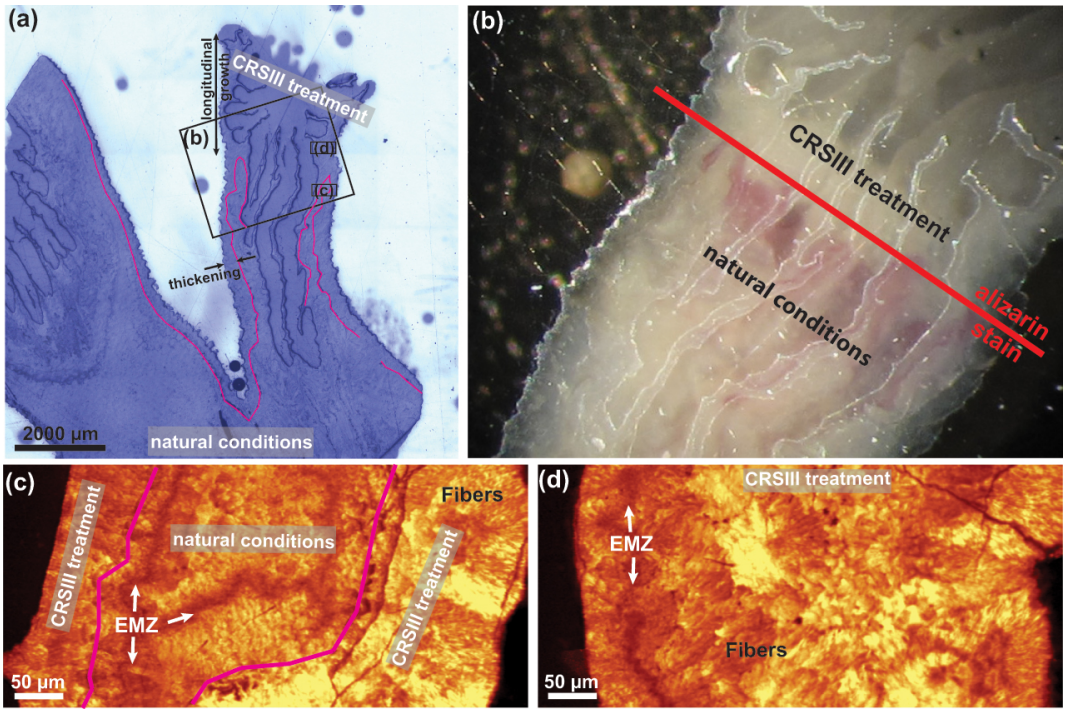

Figure 2. (a) *Lophelia pertusa* cut in longitudinal plane through an old and younger colony branch. Pink line outlines the position of the staining lines and separates the skeleton grown under natural and high CO_2 treatment conditions (CRSIII $pCO_2 = 982$). **(b)** Close-up of side branch and location of the staining edge above all skeleton was formed during treatment conditions. **(c, d)** Raman map of the intensity distribution of the main aragonite peak (symmetric stretch, 1085 cm^{-1}) reveals the early mineralization zone (EMZ), the primary skeleton and the area of secondary thickening precipitated for both natural and treatment conditions.

related to linear extension of a polyp (Fig. S2) nor the location (Form A., personal communication, 2015).

3 Results

The main growing edge outlined by the Alizarin staining lines marks the border to the experimentally precipitated distal skeleton (Fig. 2). In microscopic images, the staining line is only visible at the main growing edge (Fig. 2b), whereas in Raman fluorescence maps the outer skeletal surface before the start of the experiment can be traced over the entire colony (Figs. 2, 3). The Raman maps clearly display the orientation of the skeletal fibres and the location of the early mineralization zone (EMZ: Cuif and Dauphin, 2005, or rapid accretion front, RAF: Stolarski, 2003) and were used to compare skeletal formation before and during experimental conditions (Fig. 2c, d). At the macromorphological level, i.e. the arrangement of the main skeleton entities (EMZ and fibres), no notable difference between the natural and high pCO_2 sample can be detected (Figs. 3c, d, 5, 6b).

Skeletal tomography reveals a large degree of morphological variability within the *L. pertusa* skeleton. Both the thickness of the outer wall and septa vary strongly as do the shape and length of the septa (Fig. 7). In addition, the vertical extension of newly grown material (after staining) was not even (Fig. 7). To enable a direct comparison between the natural material and that grown at high CO_2, sections were taken directly above and below the Alizarin stain (Fig. 7b). These sections show that there is no change in structure for three different pCO_2 treatments (Fig. 7c–h) which was confirmed by measurements on longitudinal polyp sections (Fig. S3). Overall thickness is slightly higher below the staining line than above (thickness ratio below/above of 1.10 ± 0.07) and range from 0.82 ($\pm$0.04), 1.14 ($\pm$0.09) to 1.32 ($\pm$0.16) for the CRSII, CRSI and CRSII, respectively (see Fig. S3).

All the samples and transects analysed for boron isotopes are summarized in Table 2. Repeated cross sections of the same corallites are reproducible (same colony and same polyp $\delta^{11}B$ mean $\pm$ SE: 26.41 ‰ $\pm$ 0.83 vs. 26.08 ‰ $\pm$ 0.61 and 27.62 ‰ $\pm$ 1.09 vs. 27.55 ‰ $\pm$ 0.57) as were transects comparing two coral polyps from the same coral colony (27.96 ‰ $\pm$ 0.48 vs. 27.62 ‰ $\pm$ 1.09). Hence, we observed consistent values within the population grown in their natural environment within error.

All transects show heterogeneity in $\delta^{11}B$ varying from $\sim$ 19.8–32.2 ‰, in particular when old branches with secondary thickening were analysed (Figs. 4, 6, S4). The variability of $\delta^{11}B$ in *L. pertusa* spans approx. 14 ‰ and reveals lower values within the primary skeleton around the EMZ 22.48 $\pm$ 1.58 ‰ (mean $\pm$ SD, see Supplement Table S1) and

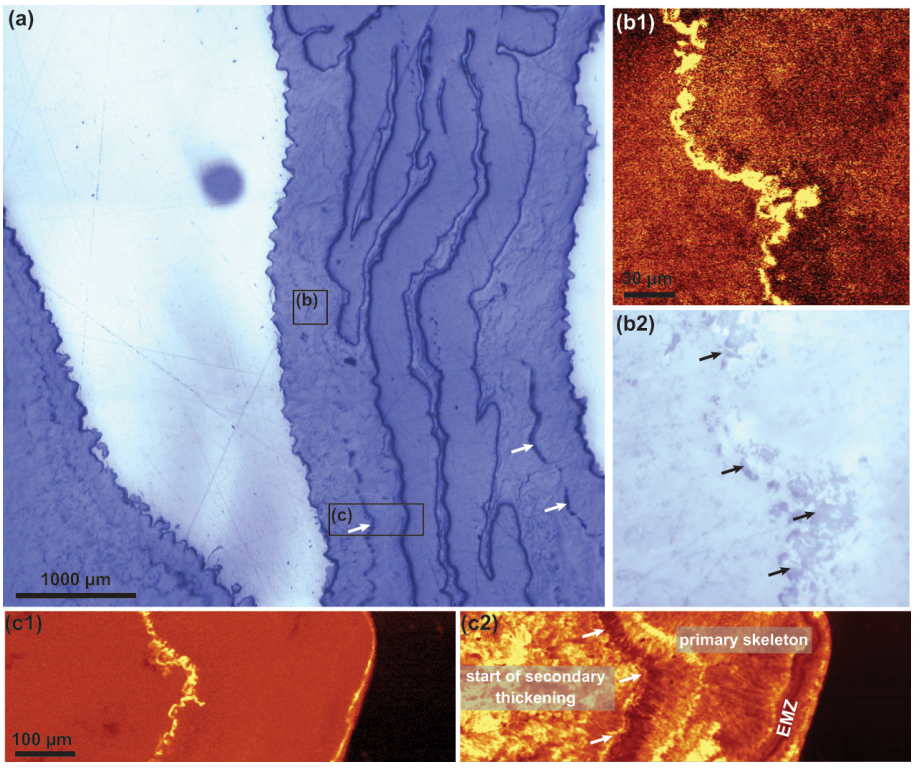

Figure 3. (a) *Lophelia pertusa* cut in longitudinal plane displays the location of Raman maps and microscopic image (50×). **(b)** Raman map of the staining line **(b1)** and the growth interruptions (black arrows) shown in the microscopic image **(b2)**. **(c)** Raman maps of the location of the staining line **(c1)** and the growth interruption seen in aragonite orientation map **(c2)**.

Table 2. Summary of skeletal boron isotopic composition (δ^{11}B; mean, standard deviation (SD) and standard error (SE)) for different transects on transversal sections of different *Lophelia pertusa* polpys (from 3 different colonies) and the corresponding pH (mean, min and max). Repeated parallel transects were performed on a few polyps. The transect cross different skeletal regions (see Figs. 4–6 and Supplement) here indicated as natural in situ grown skeleton (Nat) and/or skeleton grown during laboratory culturing conditions (CRSIII).

				δ^{11}B transcect			pH		
Colony	ind. polyp	Transect	skeletal region	mean	SD	SE	min	mean	max
I	1	1	Nat	26.41	4.09	0.83	8.80	8.85	8.90
I	1	2	Nat	26.08	3.38	0.61	8.79	8.83	8.87
II	2	3	Nat	27.96	2.56	0.48	8.92	8.95	8.98
II	3	4	Nat	27.62	5.10	1.09	8.86	8.93	9.00
II	3	5	Nat	27.55	2.55	0.57	8.89	8.92	8.96
III	4	6	CRSIII	24.81	1.40	0.29	8.76	8.78	8.80
III	4	7	CRSIII	24.74	1.57	0.31	8.75	8.77	8.79
III	4	8	Nat & CRSIII	23.70	2.02	0.41	8.65	8.68	8.70
III	5	9	Nat & CRSIII	25.44	2.75	0.54	8.75	8.79	8.82

an increase towards the outer skeletal rims (Figs. 4, 6, S4, S5). The secondary thickening is characterized by a higher δ^{11}B of 26.97 ± 4.73 ‰ compared to the primary material and slightly reduced values at opaque nucleation sites (Figs. 6, S4).

Material that was deposited along the same skeletal region has the same δ^{11}B (shown by repeated transects on several polyps; Figs. 4, 5). Transects on different polyps with similar diameter of the same colony show the same δ^{11}B (transect 3,4, Table 2). The secondary thickening has the same δ^{11}B independent of whether it was precipitated during natural or the high pCO_2 condition (26.97 ± 4.73 and 27.8 ± 1.94 ‰, respectively; Fig. 3c) corresponding to a pH_{cf} of 8.94 ± 0.15 or 8.95 ± 0.13, respectively. The sample grown only under high

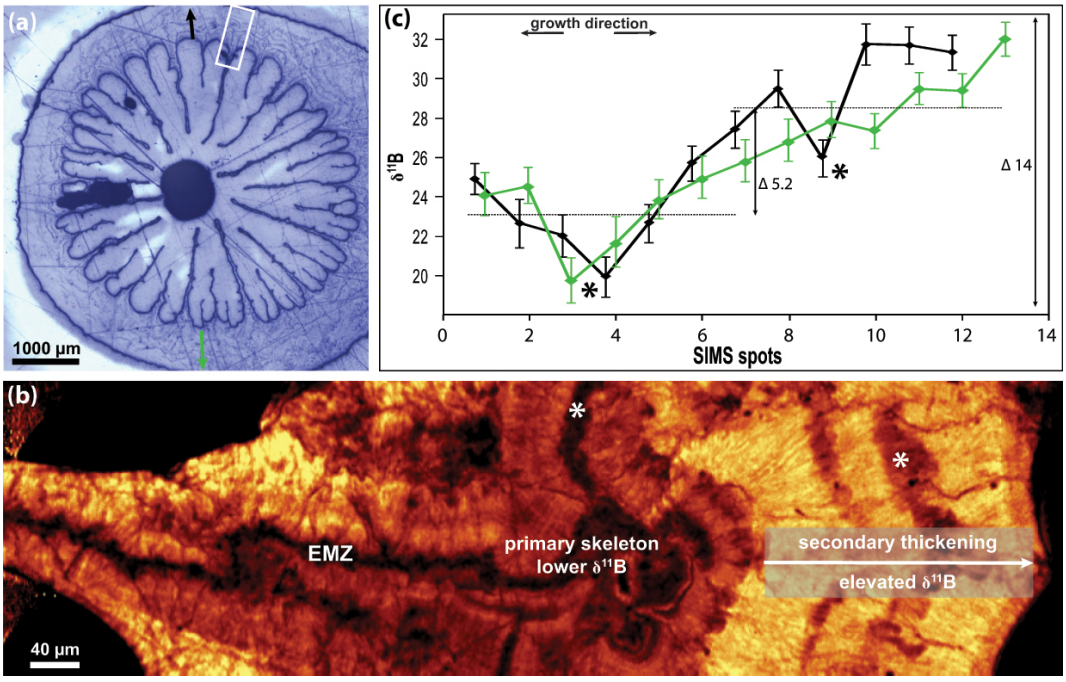

Figure 4. Side branch of *Lophelia pertusa* cut in transversal plane and prepared for Raman mapping and SIMS analysis. **(a)** Microscopic image contains the location of the Raman map and the SIMS transects. **(b)** Raman map of the intensity distribution of the main aragonite peak (symmetric stretch, 1085 cm^{-1}) reveals the early mineralization zone (EMZ), the primary skeleton and the area of secondary thickening. Asterisks mark EMZ in the primary skeleton and skeletal areas within the secondary thickening zone of potentially reduced Boron isotopic value (cf. opaque growth bands in Blamart et al., 2007 or 1°, 2° nucleation zone in Cohen et al., 2006). **(c)** $\delta^{11}B$ measured from inside to the outer coral skeletal rims (transect #1,2).

pCO_2 has slightly higher average $\delta^{11}B$ (24.52 ± 1.21 ‰) within the primary skeleton (Fig. 6) compared to primary skeleton precipitated under natural conditions. During the formation of the primary skeleton the calculated internal calcifying fluid pH_{cf} is lower than during secondary thickening (8.58 ± 0.11 vs. 9.01 ± 0.15). The primary skeleton formed during high pCO_2 conditions reveals a stronger internal pH up-regulation (8.74 ± 0.08) but still lower values than what was measured within the secondary thickening during high CO_2 conditions (8.95 ± 0.13).

4 Discussion

Lophelia pertusa has been shown to grow in undersaturated conditions. The amount of aragonite deposited under higher CO_2 was at least equivalent to that deposited under natural conditions in agreement with findings in other studies showing sustained calcification using different analytical approaches (Form and Riebesell, 2012; Hennige et al., 2014; Maier et al., 2012). As *L. pertusa* grows by both vertical extension and by thickening, measurements by buoyant weight though do not provide information on whether the morphology is affected, i.e. does the skeleton thicken or thin during low saturation or remain unchanged?

Tomographic analyses showed that the morphology of *Lophelia* skeletons is highly variable and does not change under high CO_2 even in undersaturated waters. We observed no change in the internal structure, in contrast other calcifying organisms, which show wall deformation in tube worms or coralline algae (Chan et al., 2012; Ragazzola et al., 2012). Arrangement and size of the primary skeleton, the template of size and shape of the corallite, do not change between treatments. The succession of growth bands is maintained and layers are formed even at undersaturated conditions. This finding corroborates a strong biological control on coral biomineralization. The only exception was less distinct organic layers, which might represent an impact on biomineralization in response to ocean acidification. The wider implications of a changed skeletal organic matrix need to be investigated further to understand its full implications.

A strong biological control on the biomineralization should also be expressed in its chemical composition, especially the boron isotope compositions (McCulloch et al., 2012; Hönisch et al., 2004). As deep-water corals grown in relatively stable environmental conditions, the high-resolution spatial isotopic and elemental heterogeneities suggest a biotic control that changes during growth. The isotopic heterogeneity is associated with specific skeletal regions (Blamart et al., 2007) and is also observed in other

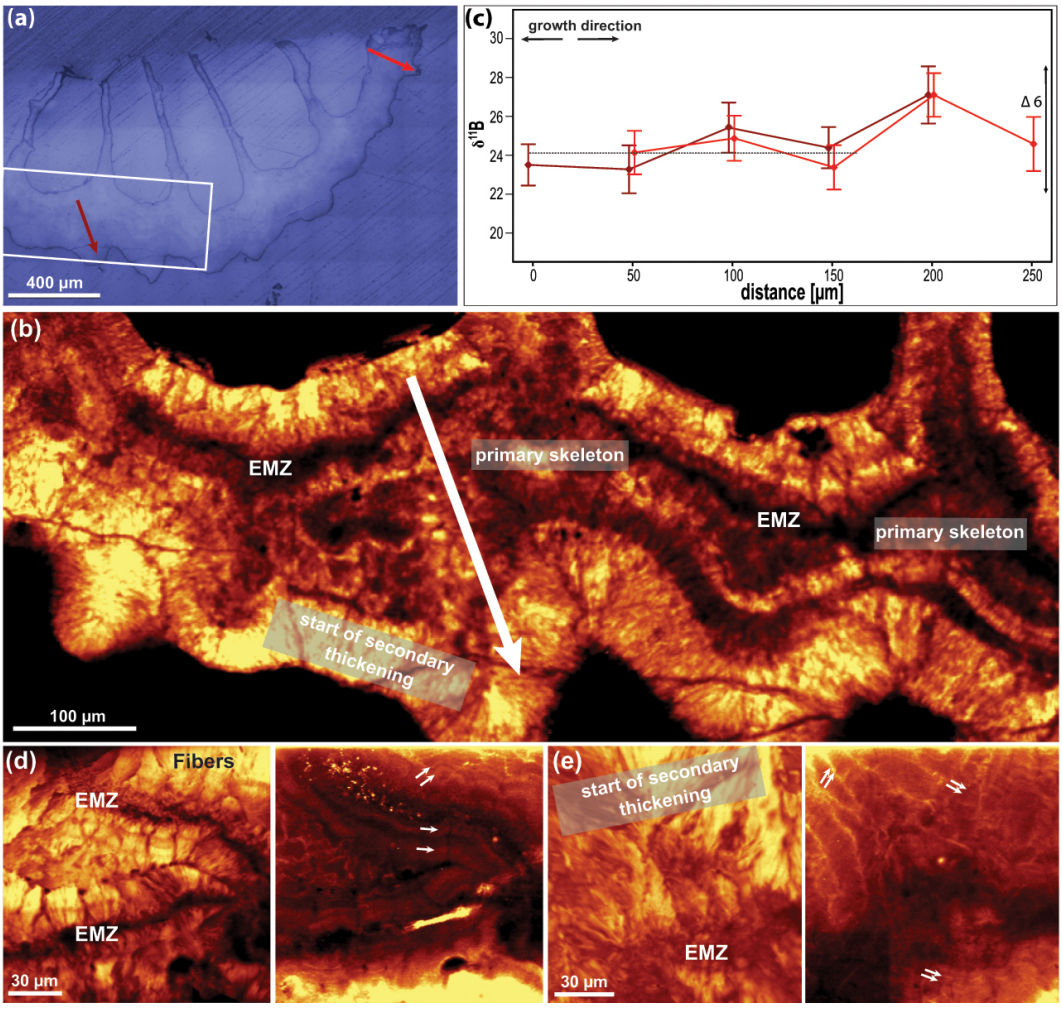

Figure 5. New branch of *Lophelia pertusa* cut above the staining line in transversal plane and prepared for Raman mapping and SIMS analysis. **(a)** Microscopic image displays the location of the Raman map and the SIMS transects. **(b)** Raman map of the intensity distribution of the main aragonite peak (symmetric stretch, 1085 cm^{-1}) reveals the early mineralization zone (EMZ), the primary skeleton and the start of secondary thickening. **(c)** $\delta^{11}B$ measured from inside to the outer coral skeletal rim (transect #6,7). **(d, e)** Raman maps of aragonite fibre orientation (left map) and fluorescence (right map) within the primary skeleton with early mineralization zone (EMZ) and with starting of the secondary thickening **(e)**. The arrows in **(d, e)** mark skeletal organic matrix bands.

isotopes, e.g. $\delta^{18}O$ (e.g. Rollion-Bard et al., 2010) and elemental ratios, e.g. Mg / Ca (e.g. Cohen et al., 2006; Krief et al., 2010). The Early Mineralization Zone (EMZ) is characterized with relatively low $\delta^{11}B$ compared to adjacent fibrous aragonite with a higher $\delta^{11}B$ and increases towards the outer wall. The EMZ is also known to have systematically lighter C and O isotopic composition by ∼ 4–5 and ∼ 8–10 ‰, respectively, compared to the fibrous aragonite part (Juillet-Leclerc et al., 2009; Rollion-Bard et al., 2010). Differences in C and O isotopes are suggested to be related to a faster growth of the EMZ suggesting that different skeletal regions are grown under different control or potentially even precipitation mechanisms. While the degree of heterogeneity with respect to boron isotopes in our samples is roughly equivalent to that of Blamart et al. (2007), the absolute values are offset by ∼ 10–14 ‰. In their study the $\delta^{11}B$ translates to a maximum pH_{cf} of approximately 10.2, while our data suggest values around 8.8 to 8.9 and agree with the bulk measurements of *L. pertusa* (McCulloch et al., 2012) and direct measurements of pH of calcifying fluids in symbiotic Scleractinian corals (Al-Horani et al., 2003) which determined values of 9.28 at light (additionally elevated by symbiont activity) and 8.13 at dark with seawater values of 8.2.

The use of $\delta^{11}B$ as pH_T proxy is based on exclusive borate incorporation. Rollion-Bard et al. (2011), by re-analysing samples from Blamart et al. (2007), suggested that both borate and boric acid are incorporated in the skeleton of *Lophelia pertusa*. In their study they observed NMR differences in skeletal boron coordination, which was used as indicator for boric acid incorporation. Considering the fraction of

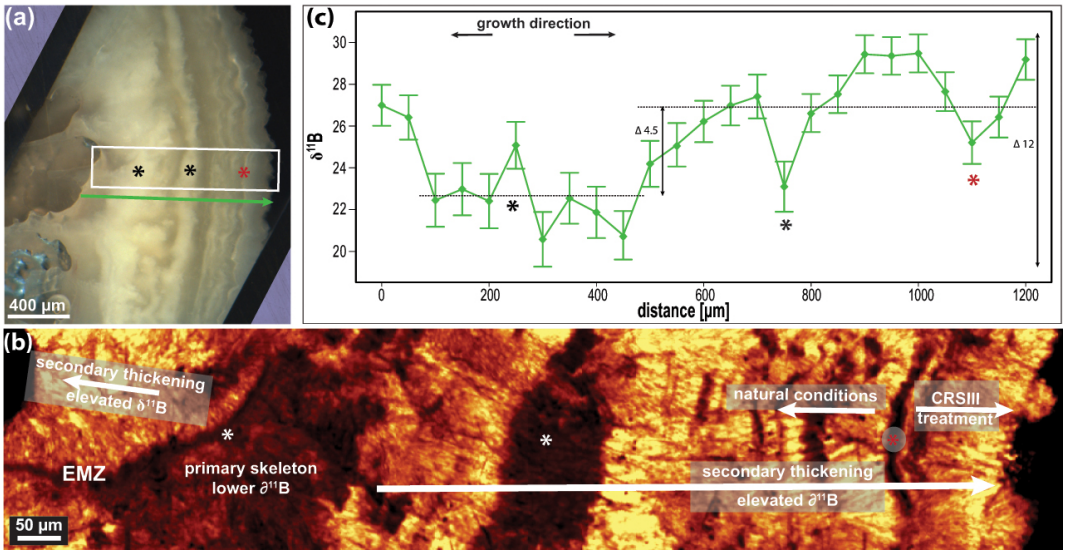

Figure 6. Old branch of *Lophelia pertusa* cut in transversal plane and prepared for Raman mapping and SIMS analysis. **(a)** Microscopic image of transversal cut through an old branch displaying the location of the Raman map and SIMS transect. **(b)** Raman map of the intensity distribution of the main aragonite peak (symmetric stretch, 1085 cm^{-1}) reveals the early mineralization zone (EMZ), the primary skeleton and the area of secondary thickening. Asterisks mark EMZ in the primary skeleton and skeletal areas within the secondary thickening zone of potentially reduced Boron isotopic value (cf. opaque growth bands in Blamart et al., 2007 or 1°, 2° nucleation zone in Cohen et al., 2006). Red asterisk marks the location of the staining line and hence, the border between growth under natural/control condition and laboratory treatment. **(c)** $\delta^{11}B$ measured in growth direction from inside to the outer coral skeletal rim (transect #9).

boric acid incorporation, they obtained pH_{cf} values similar to values obtained in other (McCulloch et al., 2012) and this study. In addition, they suggested that the EMZ incorporated a higher proportion of boric acid. In our data, we did not test whether boric acid incorporation plays a role. Our $\delta^{11}B$ to pH calculations though do not need any changes in incorporation to yield values which are comparable to bulk measurements (McCulloch et al., 2012). Applying their model to our data using $\delta^{11}B$ signature of the EMZ, the same individual would incorporate very different proportions of boric acid which is not likely given the broad range of literature on boron in corals in general. Therefore, we question this variable boric acid incorporation hypothesis.

Our interpretations are based on the internal pH_{cf} regulation calcification model (McCulloch et al., 2012) which assumes that the pH_{cf} is offset from seawater pH_T. McCulloch et al. (2012) reported a decrease in $\delta^{11}B$ with decreasing pH_T in several cold-water coral species including *L. pertusa*. They suggested that biological pH_{cf} up-regulation determines the calcification response as described also for tropical corals (Holcomb et al., 2014). In contrast, we find similar growth rates between pCO_2 treatments (Form and Riebesell, 2012) and similar $\delta^{11}B$ values (within a 0.3 pH unit error) which questions a decreasing internal pH_{cf} (Anagnostou et al., 2012; McCulloch et al., 2012).

If our interpretation of maintenance of internal pH_{cf} within the secondary skeleton is correct it suggests that pH regulation can be decoupled from external seawater pH_T and is a mechanism to explain the cold-water coral resilience. There are a number of parameters underreported in most acidification studies which might explain the difference in our findings. For example it has been suggested for a range of organisms that given a sufficient food supply, calcification can be maintained despite low saturation state (Schoepf et al., 2013; Thomsen et al., 2013). One possible explanation why we did not see a difference between treatments and the natural environment could be that food was provided in higher amounts than other studies on *Lophelia* and hence additional energy might have been available to support calcification. If this is the case than limited food availability might have a strong impact on the ability to regulate the internal pH and *Lophelia* growth (Rodolfo-Metalpa et al., 2015). Respiration rates of *Lophelia* were observed to decline (Hennige et al., 2014; Form and Riebesell, 2012) or unchanged (Maier et al., 2013) under elevated pCO_2 suggesting that other energy sources, e.g. lipids, were used to maintain growth assuming other metabolic processes remained constant. Unfortunately, our growth experiments did not monitor whether reduced respiration changes the availability of energy reserves or tissue biomass between the treatments and presents an important scope for a new study of the physiological consequences of pH_{cf} up-regulation and associated energy requirements.

We have found indications of changes in the organic matrix (OM). These less distinct OM bands could be an important step in biomineralization compromised under ocean acidification. In a tropical coral, OM production has been

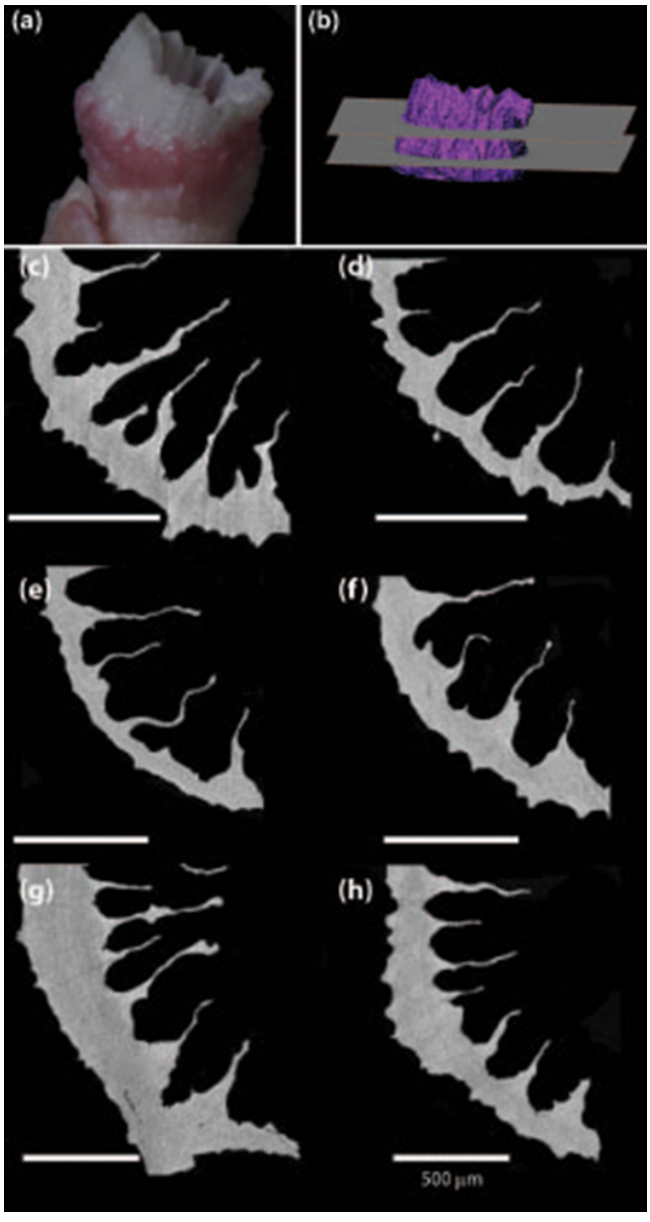

Figure 7. (a) Polyp with Alizarin stain and **(b)** reconstructed SRXTM 3D virtual model. This comparison allowed the virtual polyp to be sectioned below (left panel) and above (right panel) the Alizarin stain. Virtual SXRTM cross-sections of polyps for different pCO_2 treatment 604 **(c, d)**, 778 **(e, f)** and 982 µatm **(g, h)**.

found to be affected by both up and down regulation of certain OM protein encoding genes (Moya et al., 2012), which might result in changes in the quality of the OM. The layered growth of biogenic organisms is a prominent feature (Cuif and Dauphin, 2005) and suggests a strong biological control of growth. Thus, a less clear banding could indicate that OM formation is compromised. However, further studies are necessary to better characterize the role, function and importance of skeletal organic layers.

In conclusion, the lack of sensitivity of *L. pertusa* to changes in pCO_2 in growth, mineralogy and boron isotopes corroborates their strong biological control over biomineralization that is not easily disturbed under elevated pCO_2 conditions. Our results raise a number of questions: (1) can energy be reallocated to up-regulate the internal pH_{cf} to a suitable level which would complicate the applicability of *Lophelia skeletons* $\delta^{11}B$ record as a paleo-pH proxy given the small ranges of pH difference studies often aim to resolve and (2) the role of OM production and quality need to be considered to improve our understanding of cold-water coral biomineralization and their response to acidification.

The Supplement related to this article is available online at doi:10.5194/bg-12-6869-2015-supplement.

Author contributions. A. Form provided the specimens from the culturing experiment. M. Wall, L. C. Foster, F. Ragazzola and D. N. Schmidt collected the data. M. Wall, L. C. Foster, D. N. Schmidt, F. Ragazzola and A. Form analysed the data. M. Wall, L. C. Foster, F. Ragazzola wrote the paper, and all authors (M. Wall, L. C. Foster, F. Ragazzola, D. N. Schmidt and A. Form) contributed to the final text and figures.

Acknowledgements. This study is a contribution to the BIOACID joint project, funded by the German Ministry of Research and Technology and EPOCA. The tomographic analyses were performed on the TOMCAT beamline at the Swiss Light Source (SLS), Paul Scherrer Institut, Villigen, Switzerland (SLS grant Agreement Number no. 20110822). The staff at EMMAC are thanked for their assistance with analyses, supported by a small research grant from the Royal Society. We are grateful to Federica Marone at the Swiss Light Source whose outstanding efforts have made these experiments possible. MW has received funding from the FP7-PEOPLE-2007-1-1-ITN Marie Curie Action: CalMarO (Calcification by Marine Organisms, Grant number: 215157) and BIOACID II (Grant number: FKZ 03F0655A). L. C. Foster acknowledges support from the Holmes Fellowship and NERC grant NE/F017383/1. F. Ragazzola is supported by Leverhulme Research Grant and DNS via a URF from the Royal Society.

The article processing charges for this open-access publication were covered by a Research Centre of the Helmholtz Association.

Edited by: W. Kiessling

References

Adkins, J. F., Boyle, E. A., Curry, W. B., and Lutringer, A.: Stable isotopes in deep-sea corals and a new mechanism for "vital effects", Geochem. Cosmochem. Ac., 67, 1129–1143, 2003.

Al-Horani, F. A., Al-Moghrabi, S. M., and de Beer, D.: The mechanism of calcification and its relation to photosynthesis and respiration in the scleractinian coral Galaxea fascicularis, Mar. Biol., 142, 419–426, 2003.

Anagnostou, E., Huang, K., You, C., Sikes, E. L., and Sherrell, R. M.: Evaluation of boron isotope ratio as a pH proxy in the deep sea coral Desmophyllum dianthus?: Evidence of physiological pH adjustment, Earth Planet. Sci. Lett., 349/350, 251–260, 2012.

Bates, N. R., Best, M. H. P., Neely, K., Garley, R., Dickson, A. G., and Johnson, R. J.: Detecting anthropogenic carbon dioxide uptake and ocean acidification in the North Atlantic Ocean, Biogeosciences, 9, 2509–2522, doi:10.5194/bg-9-2509-2012, 2012.

Blamart, D., Rollion-Bard, C., Meibom, A., Cuif, J.-P., Juillet-Leclerc, A., and Dauphin, Y.: Correlation of boron isotopic composition with ultrastructure in the deep-sea coral *Lophelia pertusa*: Implications for biomineralization and paleo-pH, Geochemistry, Geophys. Geosyst., 8, 1–11, 2007.

Chalker, B. E. and Taylor, D. L.: Light-enhanced calcification, and the role of oxidative phosphorylation in calcification of the coral Acropora cervicornis, Proc. Biol. Sci., 190, 323–331, 1975.

Chan, V. B. S., Li, C., Lane, A. C., Wang, Y., Lu, X., Shih, K., Zhang, T., and Thiyagarajan, V.: CO_2-driven ocean acidification alters and weakens integrity of the calcareous tubes produced by the serpulid tubeworm, Hydroides elegans, PLoS One, 7, e42718, doi:10.1371/journal.pone.0042718, 2012.

Cohen, A. L., Gaetani, G. A., Lundälv, T., Corliss, B. H., and George, R. Y.: Compositional variability in a cold-water scleractinian, Lophelia pertusa?: New insights into "vital effects", Geochemistry, Geophys. Geosyst., 7, Q12004, doi:10.1029/2006GC001354, 2006.

Cuif, J.-P. and Dauphin, Y.: The two-step mode of growth in the scleractinian coral skeletons from the micrometre to the overall scale, J. Struct. Biol., 150, 319–331, 2005.

Davies, A. J. and Guinotte, J. M.: Global habitat suitability for framework-forming cold-water corals, PLoS One, 6, e18483, doi:10.1371/journal.pone.0018483, 2011.

Dickson, A. G.: Standard potential of the reaction: AgCl(s) + 1/2H2(g) = Ag(s) + HCl(aq) and the standard acidity constant of the ion HSO-4 in synthetic seawater from 273/15 to 318.15, K. J. Chem. Thermodyn., 22, 113–127, 1990.

Farmer, J. R., Hönisch, B., Robinson, L. F., and Hill, T. M.: Effects of seawater-pH and biomineralization on the boron isotopic composition of deep-sea bamboo corals, Geochim. Cosmochim. Ac., 155, 86–106, 2015.

Feely, R. a, Sabine, C. L., Lee, K., Berelson, W., Kleypas, J., Fabry, V. J., and Millero, F. J.: Impact of anthropogenic CO_2 on the $CaCO_3$ system in the oceans, Science, 305, 362–366, 2004.

Form, A. U. and Riebesell, U.: Acclimation to ocean acidification during long-term CO_2 exposure in the cold-water coral Lophelia pertusa, Glob. Chang. Biol., 18, 843–853, 2012.

Fosså, J. H., Mortensen, P. B., and Furevik, D. M.: The deep-water coral Lophelia pertusa in Norwegian waters?: distribution and fishery impacts, Hydrobiologia, 471, 1–12, 2002.

Foster, G. L., Pogge von Strandmann, P. a. E., and Rae, J. W. B.: Boron and magnesium isotopic composition of seawater, Geochemistry, Geophys. Geosyst., 11, Q08015, doi:10.1029/2010GC003201, 2010.

Genin, A., Dayton, P. K., Lonsdale, P. F., and Spiess, F. N.: Corals on seamount peaks provide evidence of current acceleration over deep-sea topography, Nature, 322, 59–61, 1986.

Guinotte, J. M. and Fabry, V. J.: Ocean acidification and its potential effects on marine ecosystems, Ann. N. Y. Acad. Sci., 1134, 320–342, 2008.

Hemming, N. G. and Hanson, G. N.: Boron isotopic composition and concentration in modern marine carbonates, Geochim. Cosmochim. Ac., 56, 537–543, 1992.

Hennige, S. J., Wicks, L. C., Kamenos, N. a., Bakker, D. C. E., Findlay, H. S., Dumousseaud, C., and Roberts, J. M.: Short-term metabolic and growth responses of the cold-water coral Lophelia pertusa to ocean acidification, Deep-Sea Res. Pt. II, 99, 27–35, 2014.

Henry, L.-A. and Roberts, J. M.: Biodiversity and ecological composition of macrobenthos on cold-water coral mounds and adjacent off-mound habitat in the bathyal Porcupine Seabight, NE Atlantic, Deep-Sea Res. Pt. I, 54, 654–672, 2007.

Holcomb, M., Venn, a a, Tambutté, E., Tambutté, S., Allemand, D., Trotter, J., and McCulloch, M.: Coral calcifying fluid pH dictates response to ocean acidification, Sci. Rep., 4, 5207, doi:10.1038/srep05207, 2014.

Hönisch, B., Hemming, S., Grottoli, A. G., Amat, A., Hanson, G. N., and Bijma, J.: Assessing scleractinian corals as recorders for paleo-pH: Empirical calibration and vital effects, Geochim. Cosmochim. Ac., 68, 3675–3685, 2004.

Juillet-Leclerc, A., Reynaud, S., Rollion-Bard, C., Cuif, J.-P., Dauphin, Y., Blamart, D., Ferrier-Pagès, C., and Allemand, D.: Oxygen isotopic signature of the skeletal microstructures in cultured corals?: Identification of vital effects, Geochem. Cosmochem. Ac., 73, 5320–5332, 2009.

Kasemann, S. S., Schmidt, D. N., Bijma, J., and Foster, G. L.: In situ boron isotope analysis in marine carbonates and its application for foraminifera and palaeo-pH, Chem. Geol., 260, 138–147, 2009.

Klochko, K., Kaufman, A. J., Yao, W., Byrne, R. H., and Tossell, J. a.: Experimental measurement of boron isotope fractionation in seawater, Earth Planet. Sci. Lett., 248, 276–285, 2006.

Krief et al Krief, S., Hendy, E. J., Fine, M., Yam, R., Meibom, A., Foster, G. L., and Shemesh, A.: Physiological and isotopic responses of scleractinian corals to ocean acidification, Geochim. Cosmochim. Ac., 74, 4988–5001, 2010.

Lavigne, H. and Gattuso, J.: Seacarb: seawater carbonate chemistry with R, http://CRAN.R-project.org/package=seacarb, 2010.

Maier, C., Hegeman, J., Weinbauer, M. G., and Burg, D.: Calcification of the cold-water coral Lophelia pertusa under ambient and reduced pH, 1, 1671–1680, 2009.

Maier, C., Watremez, P., Taviani, M., Weinbauer, M. G., and Gattuso, J. P.: Calcification rates and the effect of ocean acidification on Mediterranean cold-water corals, Proc. Biol. Sci., 279, 1716–1723, 2012.

Maier, C., Bils, F., Weinbauer, M. G., Watremez, P., Peck, M. A., and Gattuso, J.-P.: Respiration of Mediterranean cold-water corals is not affected by ocean acidification as projected for the end of the century, Biogeosciences, 10, 5671–5680, doi:10.5194/bg-10-5671-2013, 2013.

McCulloch, M., Trotter, J., Montagna, P., Falter, J., Dunbar, R., Freiwald, A., Försterra, G., López Correa, M., Maier, C., Rüggeberg, A., and Taviani, M.: Resilience of cold-water scleractinian corals

to ocean acidification: Boron isotopic systematics of pH and saturation state up-regulation, Geochim. Cosmochim. Ac., 87, 21–34, 2012.

Melbourne, L. A., Griffin, J., Schmidt, D. N., and Rayfield, E. J.: Potential and limitations of finite element modelling in assessing structural integrity of coralline algae under future global change, Biogeosciences, 12, 5871–5883, doi:10.5194/bg-12-5871-2015, 2015.

Mienis, F., De Stigter, H. C., White, M., Duineveld, G., De Haas, H., and Van Weering, T. C. E.: Hydrodynamic controls on cold-water coral growth and carbonate-mound development at the SW and SE Rockall Trough Margin, NE Atlantic Ocean, Deep-Sea Res. Pt. I, 54, 1655–1674, 2007.

Mortensen, P. B. and Rapp, H. T.: Oxygen and carbon isotope ratios related to growth line patterns in skeletons of *Lophelia pertusa (L.)* (*Anthozoa, Scleractinia*): Implicaitons for determination of linear extension rates, Sarsia, 83, 433–446, 1998.

Moya, a, Huisman, L., Ball, E. E., Hayward, D. C., Grasso, L. C., Chua, C. M., Woo, H. N., Gattuso, J.-P., Forêt, S., and Miller, D. J.: Whole transcriptome analysis of the coral Acropora millepora reveals complex responses to CO_2-driven acidification during the initiation of calcification, Mol. Ecol., 21, 2440–2454, 2012.

Orr, J. C., Fabry, V. J., Aumont, O., Bopp, L., Doney, S. C., Feely, R. a, Gnanadesikan, A., Gruber, N., Ishida, A., Joos, F., Key, R. M., Lindsay, K., Maier-Reimer, E., Matear, R., Monfray, P., Mouchet, A., Najjar, R. G., Plattner, G.-K., Rodgers, K. B., Sabine, C. L., Sarmiento, J. L., Schlitzer, R., Slater, R. D., Totterdell, I. J., Weirig, M.-F., Yamanaka, Y., and Yool, A.: Anthropogenic ocean acidification over the twenty-first century and its impact on calcifying organisms, Nature, 437, 681–686, 2005.

Pörtner, H. O., Karl, D., Boyd, P. W., Cheung, W., Lluch-Cota, S. E., Nojiri, Y., Schmidt, D. N., and Zavialov, P.: Ocean systems, in: IPCC WGII, edited by: Field, C. B., Barros, V. R., Dokken, D. J., Mach, K. J., Mastrandrea, M. D., Bilir, T. E., Chatterjee, M., Ebi, K. L., Estrada, Y. O., Genova, R. C., Girma, B., Kissel, E. S., Levy, A. N., MacCracken, S., Mastrandrea, P. R., and White, L. L., Cambridge University Press, Cambridge, United Kingdom and New York, NY, USA, 411–484, 2014.

Rae, J. W. B., Foster, G. L., Schmidt, D. N., and Elliott, T.: Boron isotopes and B / Ca in benthic foraminifera: Proxies for the deep ocean carbonate system, Earth Planet. Sci. Lett., 302, 403–413, 2011.

Ragazzola, F., Foster, L. C., Form, A., Anderson, P. S. L., Hansteen, T. H., and Fietzke, J.: Ocean acidification weakens the structural integrity of coralline algae, Glob. Chang. Biol., 18, 2804–2812, 2012.

Ries, J. B.: A physicochemical framework for interpreting the biological calcification response to CO_2-induced ocean acidification, Geochim. Cosmochim. Ac., 75, 4053–4064, 2011.

Ries, J. B., Cohen, a. L., and McCorkle, D. C.: Marine calcifiers exhibit mixed responses to CO_2-induced ocean acidification, Geology, 37, 1131–1134, 2009.

Roberts, M., Henry, L.-A., Long, D., and Hartley, J. P.: Cold-water coral reef frameworks and enhanced megafaunal diversity on the Hatton Bank, NE Atlantic, Facies, 54, 1297–316, 2008.

Rodolfo-Metalpa, R., Montagna, P., and Aliani, S.: Calcification is not the Achilles heel of cold-water corals in an acidifying ocean, Glob. Change Biol., 2, 2238–2248, 2015.

Rollion-Bard, C., Blamart, D., Cuif, J.-P., and Dauphin, Y.: In situ measurements of oxygen isotopic composition in deep-sea coral, *Lophelia pertusa*: Re-examination of the current geochemical models of biomineralization, Geochim. Cosmochim. Ac., 74, 1338–1349, 2010.

Rollion-Bard, C., Blamart, D., Trebosc, J., Tricot, G., Mussi, A., and Cuif, J.-P.: Boron isotopes as pH proxy?: A new look at boron speciation in deep-sea corals using 11 B MAS NMR and EELS, Geochem. Cosmochem. Ac., 75, 1003–1012, 2011.

Schoepf, V., Grottoli, A. G., Warner, M. E., Cai, W.-J., Melman, T. F., Hoadley, K. D., Pettay, D. T., Hu, X., Li, Q., Xu, H., Wang, Y., Matsui, Y., and Baumann, J. H.: Coral energy reserves and calcification in a high-CO_2 world at two temperatures, PLoS One, 8, e75049, doi:10.1371/journal.pone.0075049, 2013.

Stampanoni, M., Groso, a., Isenegger, a., Mikuljan, G., Chen, Q., Bertrand, a., Henein, S., Betemps, R., Frommherz, U., Böhler, P., Meister, D., Lange, M., Abela, R., and Boehler, P.: Trends in synchrotron-based tomographic imaging: the SLS experience, Dev. X-Ray Tomogr. V, 6318, 63180M–63180M–14, doi:10.1117/12.679497, 2006.

Stolarski, J.: Three – dimensional micro – and nanostructural characteristics of the scleractinian coral skeleton?: A biocalcification proxy, Acta Palaeontol. Pol., 48, 497–530, 2003.

Thomsen, J., Casties, I., Pansch, C., Körtzinger, A., and Melzner, F.: Food availability outweighs ocean acidification effects in juvenile Mytilus edulis: laboratory and field experiments, Glob. Chang. Biol., 19, 1017–1027, 2013.

Trotter, J., Montagna, P., McCulloch, M., Silenzi, S., Reynaud, S., Mortimer, G., Martin, S., Ferrier-Pagès, C., Gattuso, J.-P., and Rodolfo-Metalpa, R.: Quantifying the pH "vital effect" in the temperate zooxanthellate coral Cladocora caespitosa: Validation of the boron seawater pH proxy, Earth Planet. Sci. Lett., 303, 163–173, 2011.

Venn, A. A., Tambutté, E., Holcomb, M., Laurent, J., Allemand, D., and Tambutté, S.: Impact of seawater acidification on pH at the tissue – skeleton interface and calcification in reef corals, Proc. Natl. Acad. Sci. USA, 110, 1634–1639, 2013.

Wainright, S. A.: Studies of the mineral phase of coral skeleton, Exp. Cell Res., 34, 213–230, 1964.

Wall, M. and Nehrke, G.: Reconstructing skeletal fiber arrangement and growth mode in the coral *Porites lutea* (Cnidaria, Scleractinia): a confocal Raman microscopy study, Biogeosciences, 9, 4885–4895, doi:10.5194/bg-9-4885-2012, 2012.